Quasibound states in long-range alkali dimers: Grid method calculations

Olivier Dulieu
Laboratoire Aimé Cotton, Université Paris-Sud, Bâtiment 505, F-91405 Orsay Cedex, France

Ronnie Kosloff
Department of Physical Chemistry and the Fritz Haber Research Center, the Hebrew University, Jerusalem 91904, Israel

Françoise Masnou-Seeuws
Laboratoire Aimé Cotton, Université Paris-Sud, Bâtiment 505, F-91405 Orsay Cedex, France

Goran Pichler
Institute of Physics, P.O. Box 304, HR-10000 Zagreb, Croatia

(Received 28 May 1997; accepted 22 September 1997)

A local minimum is found in the 0_g^+ long range potential curves of the K_2 and Rb_2 alkali dimers. This well-of magnitude $42\,cm^{-1}$ for K_2 and $93\,cm^{-1}$ for Rb_2—is located above the first $ns+n^2P_{3/2}$ dissociation limit and metastable states could be populated using laser light blue detuned compared to the resonance line. To compute the previously unknown energies and lifetimes of these quasibound states, two grid methods are employed. One method is based on diagonalizing a Fourier grid Hamiltonian, the other uses a propagation technique in imaginary time to filter out vibrational eigenfunctions. Equivalent results are given by both methods. Then the lifetimes are extracted from the correlation function obtained by propagation in real time of these numerical vibrational wave functions. The methods are employed both in adiabatic representation with one electronic potential curve and in diabatic representation with two potential curves. Two quasibound states are found for K_2, and three for Rb_2 above seven stable bound states. Their lifetimes vary from 20 ps to 3 ns. © *1997 American Institute of Physics.* [S0021-9606(97)02848-1]

I. INTRODUCTION

Recent progress in laser cooling of atoms has made possible collision experiments at ultracold temperatures, opening the way for detailed studies of long-range interatomic potentials.[1–5] Indeed, photoassociation spectroscopy (PAS) within a cold atom sample now provides accurate data for loosely bound rovibrational states of diatomic molecules. For such states, the vibrational motion extends to relative distances between the two atoms up to several hundreds of atomic units ($1\text{ a.u.}=a_0=5.291\,77\times 10^{-11}$ m). Most experimental results have been obtained for the first excited states of the alkali dimers $M_2=Li_2$, Na_2, K_2, Rb_2, dissociating into $M(ns)+M(np^2P_{1/2,3/2})$, where ns and np are the ground state and the first excited state of the alkali atom. Starting usually from a continuum state of u symmetry, a rovibrational level of an attractive molecular potential curve of g symmetry is populated by absorption of a photon with a frequency detuned to the red from the atomic transition. Detailed information can then be deduced for the corresponding long-range potentials (typically for distances larger than $20a_0$), where the resonant dipole–dipole interaction between the atoms is the dominant electrostatic term and combines with fine structure or hyperfine structure interaction. The existence of so-called pure long-range molecules has been predicted by Stwalley *et al.*[6] using potential curves calculated by Movre and Pichler.[7] Due to the competition of the various interaction terms, long-range wells containing several bound levels may exist at distances much larger than the typical chemical bond. Up to now, their existence has been demonstrated for Na_2,[8,9] K_2,[5] and Rb_2.[10]

Some studies using laser light detuned to the blue from the atomic resonance have been recently reported, causing the excitation of long-range molecular states with repulsive potential curves. They result in the suppression of the collisions at ultracold temperatures (also called optical shielding), demonstrated in Na_2,[11,12] in Rb_2,[13,14] and in rare-gas species.[15,16] We consider in the present work a situation where the potential curve is no longer repulsive, and has a local minimum at large distances.

There is a big gap between the range of the internuclear separation where ordinary molecular transitions occur (typically for distances $3-10a_0$) and the interatomic separations where radiative transitions occur in the long-range or pure long-range molecules: In the latter case, inner turning points of the vibrational motion are around $60a_0$ in the case of sodium and $20a_0$ in the case of cesium. Spectroscopic applications of the population of bound states in long-range wells are very promising, as many other interesting excited states can be reached once this intermediate state has been excited: Applications to two-color spectroscopy of doubly excited states of Na_2,[17,9] K_2[18] have already been performed.

In the present work we discuss the case of external wells in molecular potential curves which may arise from the competition between the spin–orbit interaction and long-range interaction converging to a R^{-3} dipole–dipole term. Those wells are located at distances where the asymptotic R^{-3} behavior is not yet reached so that *ab initio* calculations are required. We shall call those states ‘‘intermediate long-range molecules.’’ An example of such a situation is provided by the fine structure coupling between the $^1\Sigma_g^+$ and $^3\Pi_g$ Hund's

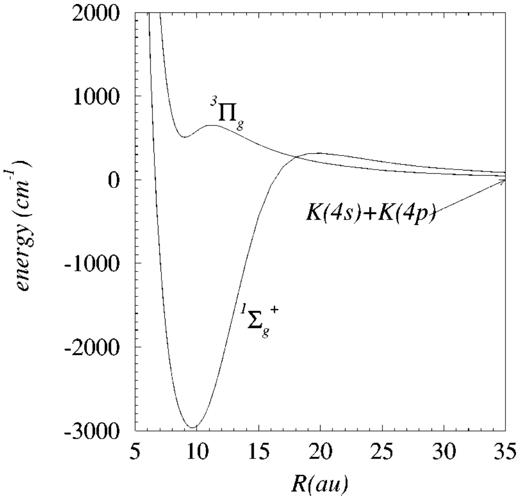

FIG. 1. $^1\Sigma_g^+$ and $^3\Pi_g$ potential curves for K_2 (fine structure neglected).

case a states dissociating into the first $ns+np$ limit of the alkali dimers, as shown for K_2 in Fig. 1. There are actually two 0_g^+ Hund's case c molecular states correlated to the $np\,^2P_{3/2}+ns\,^2S_{1/2}$ and $np\,^2P_{1/2}+ns\,^2S_{1/2}$ states of the separated atoms. Due to the avoided crossing around $17a_0$, the $0_g^+(np\,^2P_{3/2}+ns\,^2S_{1/2})$ potential curves exhibits two minima, the usual one at small internuclear separations, and a secondary one at $17.6a_0$, a typical intermediate long-range distance. The minimum of this secondary well lies above the asymptotic level of the two separated atoms. The question arises whether there are any bound levels there, and what are their lifetimes. Such states have never been observed yet, although the consequence of the avoided crossing between two 0_g^+ states has been detected in the self-broadened quasistatic blue wings of heavier alkali resonance lines.[19]

The aim of the paper is twofold:

(1) We present the results of theoretical calculations which discuss the existence of such 0_g^+ wells for the various alkali dimers and the properties (energies and lifetimes) of the quasibound vibrational levels lying in them.

(2) We discuss the theoretical methods used to compute such properties. Indeed, standard methods are often difficult to use for the determination of such loosely bound states embedded in a continuum.[20] We have checked, for the specific case of long-range molecules, the efficiency of two numerical grid methods which have recently been developed in view of other applications.

In Sec. II, we briefly discuss the potential curves for the various alkali dimers, showing that intermediate range secondary wells can indeed be observed in the cases of K_2 and Rb_2. In Sec. III, we present two different approaches to investigate the possibility for such wells to stabilize vibrational states:

(1) A time-independent method using a Fourier grid Hamiltonian method[21] and recently applied to the calculation of bound states for coupled molecular states in the short-range region.[22,23]

(2) A time-dependent method which first uses a filtering procedure based on a propagation technique in imaginary time[24–27] to filter approximate vibrational wave functions on a grid out of an initial wave packet, then propagates them in real time in order to compute their lifetime.

In Sec. IV the results are discussed in connection with possible experiments.

II. INTERMEDIATE LONG-RANGE POTENTIAL CURVES FOR THE ALKALI DIMERS

We must analyze molecular potential curves in a region where there is competition between fine structure interaction and asymptotic molecular interaction. When the spin–orbit coupling is neglected, the Hund's case a potential curves can be computed accurately by effective potential techniques up to large internuclear distances. We use the $^1\Sigma_g^+$ and $^3\Pi_g$ curves correlated to the first $ns+np$ asymptote computed in the most recent works by Magnier *et al.* for Na_2,[28] Magnier and Millié for K_2,[29] and Foucrault *et al.* for Rb_2 and Cs_2.[30] These curves are matched at large distances to the asymptotic calculations of Ref. 31. The Li_2 molecule is not considered here, as the fine structure splitting is too small to be efficient for the formation of intermediate long-range potential wells. For K_2 the curves are represented in Fig. 1: both are repulsive at large internuclear distances, the Σ curve lying above the Π curve; then, around $18a_0$, the Σ curve becomes attractive and crosses the Π curve. In an adiabatic representation, due to fine structure coupling, this crossing turns into an avoided crossing. In the present work, the electronic Hamiltonian is limited to the 2×2 subspace defined by the two Σ and Π states. We use a perturbative treatment of the fine structure coupling with an effective spin–orbit Hamiltonian where the atomic value for the fine structure constant A is introduced. This assumption is justified in the range of internuclear distances considered here, as was checked for Cs_2 by comparison to the nonperturbative results of Ref. 32. We have computed the two Hund's case c potential curves correlated to the $^2S+^2P_{1/2}$ and $^2S+^2P_{3/2}$ asymptotes by diagonalization of the effective electronic Hamiltonian. An intermediate long-range well is observable in the $0_g^+(P_{3/2})$ potential curve in Na_2, K_2, and Rb_2, as can be seen from Fig. 2 and from Table I where the position of the local minimum and neighboring local maximum are reported together with their energy position above the $^2S+^2P_{3/2}$ asymptote. It should be noted that when they exist, the wells are very shallow: $40\ \mathrm{cm}^{-1}$ for Na_2, $42\ \mathrm{cm}^{-1}$ for K_2, and $93\ \mathrm{cm}^{-1}$ for Rb_2. Due to the large value of the atomic fine structure in cesium, and with the present accuracy of the calculations it is not possible to assert whether there is a real well or a shoulder in the potential.

We have searched for the possible bound levels lying within these wells by performing both single-channel and two-channel calculations. In the first case, we introduce only the potential energy $V(R)$ of the upper $0_g^+(P_{3/2})$ adiabatic curve. In the two-channel calculations, we have used a di-

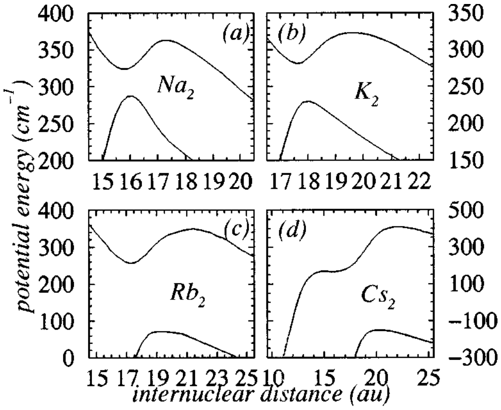

FIG. 2. 0_g^+ adiabatic potential curves correlated to the first $S_{1/2}+P_j$ ($j=1/2,3/2$) asymptotes of alkali dimers.

abatic representation, where we define a 2×2 potential matrix $V_{ij}(R)$:

$$\begin{pmatrix} V_\Sigma & A/\sqrt{2} \\ A/\sqrt{2} & V_\Pi - A/2 \end{pmatrix} \tag{2.1}$$

containing the $^1\Sigma_g^+$ and $^3\Pi_g$ energies V_Σ and V_Π as diagonal elements, and the spin–orbit coupling as an off-diagonal element and correction to the V_Π energy. We have taken the atomic values $A_{\mathrm{K}}=38.4\ \mathrm{cm}^{-1}$ and $A_{\mathrm{Rb}}=158.4\ \mathrm{cm}^{-1}$ for the fine structure constant A of the two molecular states.

Alternatively, the two-channel calculations could have been performed in an adiabatic representation considering the upper and lower 0_g^+ curves coupled by radial coupling. In the present study, we assume that there is no coupling between the rotation motion of the molecule and the electronic motion.

III. QUASIBOUND STATE CALCULATIONS: DESCRIPTION OF THE METHODS, DETERMINATION OF THE ENERGIES AND LIFETIMES

As can be seen from Table I, the minimum in the outer well for K_2 and Rb_2, described in Sec. II, lies above the $np\,^2P_{3/2}+ns\,^2S_{1/2}$ and $np\,^2P_{1/2}+ns\,^2S_{1/2}$ dissociation limits, so that the bound states are embedded in *two* dissociation continua, and should be considered as resonances. However, by performing calculations in a finite box, a bound state treatment can be implemented in a first step.

Two different grid methods are considered. In both methods, the wave functions are represented by their values on a grid of N equally spaced points, either in the coordinate space for internuclear distances, or in the momentum space through Fourier transform. The Hamiltonian operator is computed from the evaluation of the potential operator $\mathbf{V}$, diagonal in the coordinate representation and of the kinetic operator $\mathbf{T}$, diagonal in the momentum representation.

Once these approximate resonant states have been obtained they can be further refined by propagating their wave functions in real time with outgoing boundary conditions, providing a determination for their lifetime.

A. Fourier grid Hamiltonian method

The fundamental principles of the Fourier grid Hamiltonian method (FGH) are extensively described in Ref. 21. The present application is very similar to the calculations performed in Ref. 23 for the spin–orbit perturbations in the alkali dimer spectra, the only difference being that the wells are very shallow in the present case. Briefly, the potential energy operator $\mathbf{V}$—local in the coordinate space—and the kinetic energy operator $\mathbf{T}$—local in the momentum space—are represented by their mapping on a grid of N equally spaced values of internuclear distances. Each potential curve involved is described by a $N\times N$ diagonal matrix:

$$V_{ij}=V(R_i)\delta_{ij}, \quad i=1,\ldots,N, \tag{3.1}$$

while the kinetic energy is expressed as a diagonal matrix in the momentum space:

$$T_{rs}=k_r^2/2\mu\,\delta_{rs}, \quad r=1,\ldots,N, \tag{3.2}$$

where μ is the reduced mass of the system. An analytical Fourier transform yields the corresponding *nondiagonal* matrix in the coordinate representation:[33]

$$T_{ii}=\frac{\hbar^2}{4\mu L^2}\,\frac{N^2+2}{6}, \tag{3.3}$$

$$T_{ij}=(-1)^{i-j}\,\frac{\hbar^2}{4\mu L^2}\,\frac{1}{\sin^2[(i-j)\pi/N]}. \tag{3.4}$$

TABLE I. Computed properties of the outer well of the $0_g^+(P_{3/2})$ potential curve in the alkali dimers. The minimum of the well is located at distance R_e and energy E_e, with a depth D_e; the top of the barrier is located at distance R_b, and energy E_b, the height being H_b. The origin of energies is taken at the first $s+p$ limit for each dimer, so that $H_b=E_b-\Delta E_{fs}/3$.

$0_g^+(S+P_{3/2})$		Potential well			Potential barrier		
Dimer	ΔE_{fs} (cm^{-1})	R_e (a.u.)	E_e (cm^{-1})	D_e (cm^{-1})	R_b (a.u.)	E_b (cm^{-1})	H_b (cm^{-1})
Na_2	17.2	15.8	323.4	39.9	17.3	363.3	357.6
K_2	57.6	17.6	281.0	42.0	19.6	323.0	303.8
Rb_2	237.6	17.3	255.8	93.3	21.4	349.1	269.9
Cs_2	554.1	15.9	165.2	1.4	22.1	407.6	222.9

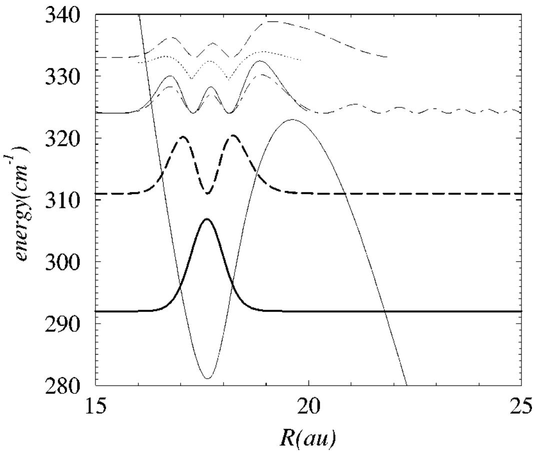

FIG. 3. Probability densities for the lowest levels in the $0_g^+(P_{3/2})$ potential curve in K_2, computed with the FGH method with one channel. The $v=0,1$ levels are drawn (thick lines) at their approximate energy. Several determinations of the $v=2$ level are given (thin lines), slightly shifted around its energy for clarity. Full line: FGH method with the [15–20 a.u.] grid; dot-dashed line: FGH method with the [6–3.0 a.u.] grid; dotted line: filtering only (see the text); dashed line: FDM.

TABLE II. Energies (in cm^{-1}) computed within a one-channel model for the $v=0,1,2$ levels in the outer well of the $0_g^+(P_{3/2})$ potential curve in K_2. The different cases are discussed in Sec. III B. The number of time steps N_τ (of 0.5 ps duration), the initial guesses ϵ for the energy, and the dispersion D (in cm^{-1}) in the filter diagonalization method (FDM) are also reported. The origin for the energies is the $4s+4p$ dissociation limit. The top of the barrier being located at 323 cm^{-1}, the $v=2$ level should be considered as a resonance.

Method		$v=0$	$v=1$	$(v=2)$
FGH				
[6–30 a.u.] grid	E	292.16	311.29	324.44
[15–20 a.u.] grid	E	292.16	311.31	324.74
Filtering				
only [$D=0.01$ cm^{-1}]	E	292.14		
	$\epsilon[N_\tau]$	0 [3]		
	E	292.15	311.27	323.20
	$\epsilon[N_\tau]$	290 [47]	310 [249]	320 [323]
FDM	E	292.15	311.27	323.23
$\epsilon=270$	D	0.006	0.014	0.14

The diagonalization of the $N\times N$ matrix (single-state calculations) or of the $2N\times 2N$ matrix (two-state calculations) provides eigenvalues corresponding either to bound states or to (discretized) continuum states. True bound states are identified by looking for those wave functions which are located within the extension of the potential well. Bound states interacting with the dissociation continuum have a small oscillating part extending toward the grid edge: this part of the wave function cannot be used for quantitative calculations, as it depends on the extension of the grid, i.e., of the discretization of the continuum; however, it allows one to identify the corresponding state as a quasibound level with a finite lifetime. The energy of such states weakly depends upon the grid extension, as will be discussed below. In contrast, the wave functions for the continuum states extend over all the grid, and the density of states or their energies markedly depend upon the size of the grid.

The accuracy of the FGH method has already been checked for single well curves of Na_2 in Ref. 23: The computed vibrational wave functions ψ_v provide rotational constants $B_v=\langle\psi_v|1/(2\mu R^2)|\psi_v\rangle$ in very good agreement with experiment. In the present work, typical results for a single state calculation using the $0_g^+(P_{3/2})$ adiabatic curve of K_2 are presented in Fig. 3. A grid with 500 points has been used, ranging from $6a_0$ to $30a_0$. The convergence of the eigenvalues is checked by varying the number of grid points, and a numerical accuracy better than 0.1 cm^{-1} is reached. All the vibrational levels of this double-well curve are obtained within such conditions. One may as well restrict the range of the grid to the outer well only, in order to save computing time and memory. Choosing a 100-point grid extending from $15a_0$ to $20a_0$, we obtain exactly the same results. This allows us to conclude that the outer well in the adiabatic $0_g^+(P_{3/2})$ curve clearly supports two bound states, easily labeled as $v=0,1$. Their energies are reported in Table II. Two determinations for a $(v=2)$-like vibrational state, mainly localized within the external well, are also shown for both grids above. The energy of this state lies slightly above the barrier, and now the shape of the wave function varies according to the grid size, as is illustrated in Fig. 3.

B. Filter diagonalization method

While the FGH method requires the evaluation of the entire Hamiltonian matrix in a large basis, the filter diagonalization method,[24–27] hereafter referred to as FDM, is designed to extract a single eigenstate or a small subset of eigenstates of the Hamiltonian within a limited energy range. An energy filter based on a Gaussian filtering procedure is used to locate the wave function in the predetermined energy range. From the filtered wave function, a Krylov space is then constructed and used as a basis for diagonalizing the Hamiltonian. We shall use the same example as in Sec. III A for a single-state calculation.

In order to obtain the ground state of our system, it was suggested in Ref. 24 to choose as an initial wave function $\psi_{\rm int}$ a Gaussian wave packet localized in the region of the minimum of the potential and to propagate it in imaginary time, $t=-i\tau$ according to

$$\psi(\tau)=e^{-\mathbf{H}\tau/\hbar}\psi_{\rm int}\equiv e^{-i\mathbf{H}t/\hbar}\psi_{\rm int}, \tag{3.5}$$

where $\mathbf{H}$ is the Hamiltonian of the system. This procedure filters out the higher energy eigenstates of $\mathbf{H}$ and as $\tau\rightarrow\infty$ only the ground state survives. Since the normalization is not conserved in this propagation scheme, it is employed repeatedly with a finite τ and the wave function is renormalized at every time step to keep the numerical calculations within the range of the computer.

In the present work we use for all states the procedure designed by Ref. 25 to obtain excited eigenstates. A Gaussian filter is selecting states in an energy region around an initial guess ϵ:

$$\psi(\tau)=e^{-4(\mathbf{H}-\epsilon)^2\tau/\hbar\Delta E}\psi_{\rm int}\equiv e^{-4i(\mathbf{H}-\epsilon)^2t/\hbar\Delta E}\psi_{\rm int}. \tag{3.6}$$

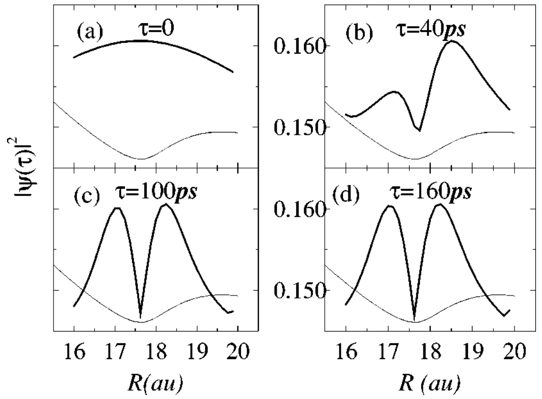

FIG. 4. Filtering sequence for the modulus of the wave function of the $v=1$ level in the outer well of the $0_g^+(P_{3/2})$ potential curve in K_2 (one channel calculation).

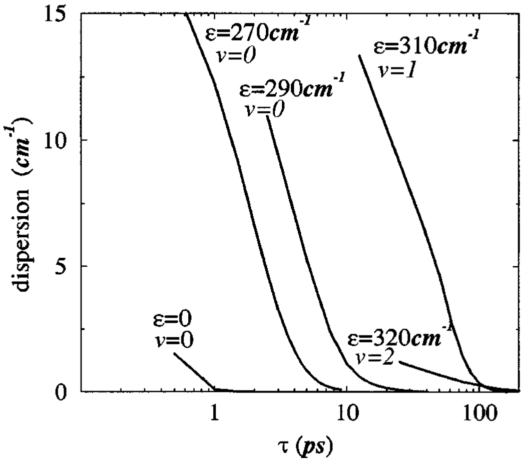

FIG. 5. Dispersion as a function of filtering time, on the energies of the $v=0,1,2$ levels in the outer well of the $0_g^+(P_{3/2})$ potential curve in K_2, after the filtering procedure (one channel calculation). All curves are truncated for low τ values for clarity.

The real parameter τ has the dimension of a time while ΔE is the energy range covered by our numerical procedure and appears as a scale factor in the propagation algorithm where the propagator is expanded by Newtonian interpolation polynomials with Chebychev sampling points.[34,35] This choice for sampling points ensures a uniform convergence in the whole spectral range of the Hamiltonian, i.e., the errors are distributed in a uniform way. This procedure can be interpreted as relaxation to the ground state of a modified Hamiltonian: $\mathbf{H}^*=4(\mathbf{H}-\epsilon)^2/\Delta E$. The quality of the result can be checked by computing the dispersion

$$D(\tau)=\sqrt{\langle\psi(\tau)|\mathbf{H}^2|\psi(\tau)\rangle-\langle\psi(\tau)|\mathbf{H}|\psi(\tau)\rangle^2}, \tag{3.7}$$

which is zero for a pure energy eigenstate, and is used as a criterion to stop the propagation process of Eq. (3.6). The rapidity of the convergence will be influenced by the value of the initial guess ϵ, relative to the final eigenenergy E. As the filtering parameter τ has the dimension of a time, we shall use a unit value $\tau_s=20\,678$ a.u., or 0.5 ps, which is well adapted to the physics of the problem.

For the single potential calculation involving the $0_g^+(P_{3/2})$ potential curve of K_2, we employed a 64-point grid extending from $R=14a_0$ to $R=22a_0$ with a mesh size $\Delta R=0.125a_0$. The initial Gaussian wave packet ψ_{int} of width $4a_0$, is centered at the minimum of the well ($R_e=17.6a_0$), and extends far outside the grid borders, in order to ensure that it will contain at least a small part of the continuum eigenstates [Fig. 4(a)]. In the momentum space, the wave packet is centered around an arbitrary (low) value of 0.01 a.u. In Fig. 4(b)–4(d) we show a typical filtering sequence for the $v=1$ level, obtained with an initial guess for the energy $\epsilon=310\ \mathrm{cm}^{-1}$ and a propagation step $\tau_s=0.5$ ps. The dispersion reaches $0.01\ \mathrm{cm}^{-1}$ after about $N_\tau=330$ time steps. In principle, the filtering procedure is sufficient to find any energy eigenstate, and the results after filtering individually the $v=0,1,2$ levels are displayed in Table II. For the $v=0,1$ levels, the results are the same as for the FGH method. In contrast, the wave function of the $v=2$ resonant level, strongly mixed with the continuum, differs from the two previous determinations (see Fig. 3) and has a very slow convergence with τ.

A repeated application will eventually lead to zero dispersion. But it has been pointed out by Neuhauser[26,36,27] that the convergence of the filtering procedure is slow. This is illustrated in Table II, and in Fig. 5: the determination of the energy of the excited levels at a given level of accuracy requires many more time steps than for the ground state energy. To speed up the convergence and to obtain at once several neighboring eigenstates, the filtering procedure is stopped after N_τ steps (or $\tau^{\mathrm{filter}}=N_\tau\tau_s$), well before reaching an accurate determination of a given vibrational level v. This yields an approximate eigenstate ψ_v^F. Then a subspace K of n_{Kryl} states is generated from the Hamiltonian $\mathbf{H}$ operating on ψ_v^F:

$$\begin{aligned}&\phi_0^K=\psi_v^F,\quad \phi_1^K=\mathbf{H}\psi_v^F,\\ &\phi_2^K=\mathbf{H}^2\psi_v^F,\ldots,\phi_{n_{\mathrm{Kryl}}-1^K}=\mathbf{H}^{n_{\mathrm{Kryl}}-1}\psi_v^F.\end{aligned} \tag{3.8}$$

The dimension n_{Kryl} of K is chosen comparable to the number of eigenstates considered. The Hamiltonian is finally diagonalized within the subspace K, after a suitable orthogonalization scheme, as for example the Gram–Schmidt procedure:

$$\begin{aligned}&\xi_0=\phi_0^K,\quad \xi_1=\phi_1^K-\langle\phi_0^K|\phi_1^K\rangle\phi_0^K,\\ &\xi_2=\phi_2^K-\langle\xi_0|\phi_2^K\rangle\xi_0-\langle\xi_1^K|\phi_2\rangle\xi_1^K,\ldots\ .\end{aligned} \tag{3.9}$$

This procedure will be efficient if the elements in K are not linearly dependent, thus requiring one to stop the filtering procedure before reaching a too low value for the dispersion D. The present procedure differs from the procedure suggested by Neuhauser but has the same effectiveness. Mathematically the procedure described by Eqs. (3.8) and (3.9) is equivalent to the Lanczos method,[37,34] but due to the use of the modified Gram–Schmidt procedure (3.9) it should be more stable. However, the size of the Krylov space is limited by the numerical instabilities generated by the Gram–Schmidt procedure, practically limiting n_{Kryl} to the range 5–12.[34]

In the present example, we have chosen a Krylov space with $n_{\mathrm{Kryl}}=5$. The energies are reported in the bottom of Table II. Through successive trails, we finally generated a ground state approximate wave function $\psi^F_{v=0}$, starting from an initial guess $\epsilon=270\ \mathrm{cm}^{-1}$, and stopping when reaching a dispersion $D=0.1\ \mathrm{cm}^{-1}$ after $N_\tau=18$ steps (or $\tau^{\mathrm{filter}}=9$ ps): The resulting dispersion on the three lowest eigenvalues of the Krylov space is then equivalent to the one obtained in the filtering-only procedure, but in a much shorter time, as the filtering procedure has not been repeated for the excited states. As mentioned previously, the $v=2$ level is less accurate as its energy is already slightly above the edge of the well. Nevertheless, the agreement with the previous FGH method is excellent (see Table II). The wave function for the $v=2$-like level is drawn in Fig. 3, and differs slightly from the FGH determinations.

C. Filtering by time propagation: Lifetimes

Due to their energy, larger than the dissociation energy of the ${}^2S+{}^2P_{3/2}$ limit, the states located in the $0_g^+(P_{3/2})$ outer potential well have a metastable character, which does not manifest itself clearly in the above procedures, because of the boundary conditions imposed by a finite grid. We must allow the metastable states obtained in the two preceeding sections to evolve freely as a function of real time t: Their wave function ψ^K, obtained from the Krylov procedure, is now propagated according to

$$\Psi(t)=e^{-i\mathbf{H}t/\hbar}\Psi^K. \tag{3.10}$$

Outgoing boundary conditions are defined by transferring the outgoing portion of the wave function to another grid.[38] Use of an imaginary absorbing potential would have the same effectiveness.[24,39,40]

Propagating the metastable wave function in real time has the effect of a time filter. The components which belong to the continuum will decay much faster than the long-lived resonance.[41] After a large enough time delay, only the resonance is left which is manifested by a wave function with a constant shape.

As a demonstration, the wave functions of the $v=0,1,2$ levels obtained above, after diagonalization within the Krylov subspace, are chosen as initial wave functions for the real time-propagation procedure. The numerical propagation scheme is the same as for the filtering procedure. The time evolution of the $v=2$ level is illustrated in Fig. 6: As expected, since this level lies above the barrier, the propagation in real time finally filters out the $v=1$ bound level. A similar time sequence may also be drawn for the $v=0,1$ levels: The shape of their wave function does not vary in time as there is no continuum components in such states.

The lifetime τ_v is deduced from the time dependence of the correlation function

$$C(t)=\langle\psi(0)|\psi(t)\rangle, \tag{3.11}$$

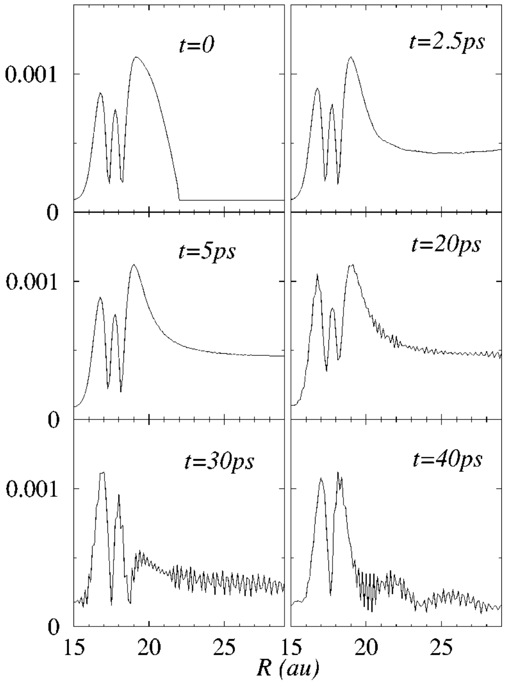

FIG. 6. Modulus of the wave function as a function of propagation time for the $v=2$ level in the outer well of the $0_g^+(P_{3/2})$ potential curve in K_2 (one channel calculation). The high frequencies oscillations are due to an abrupt cutoff of the initial wave function at the edge of the grid.

which is represented in Fig. 7 for the three $v=0,1,2$ metastable bound levels of the outer well. The decreasing exponential is clearly manifested for the three levels, so that the lifetime τ_v is readily obtained from

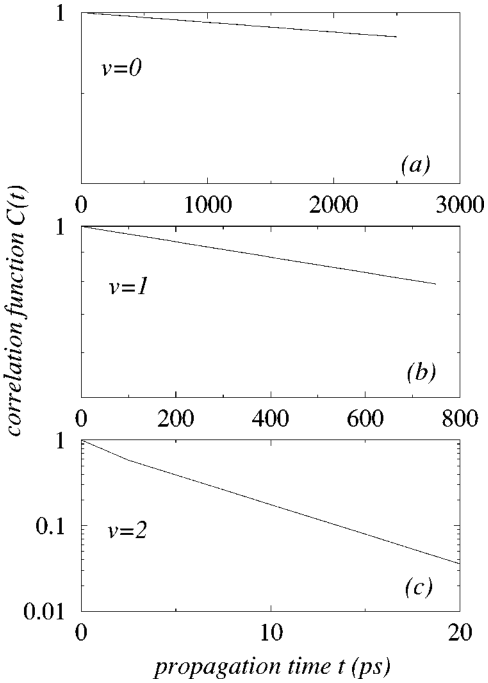

FIG. 7. Correlation function $C(t)$ (on a logarithmic scale) for the $v=0,1,2$ in the outer well of the $0_g^+(P_{3/2})$ potential curve in K_2 (one channel calculation).

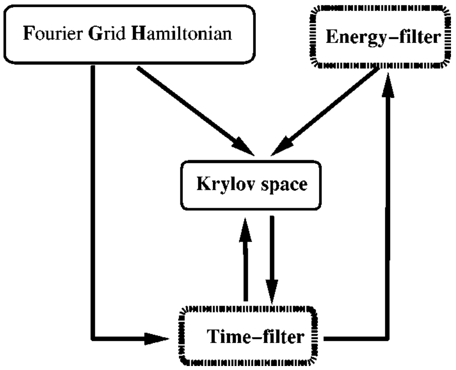

FIG. 8. Schematic description of the present methods for calculating energy and lifetime of resonant states.

$$\tau_v = -\frac{t_2 - t_1}{\log[C(t_2)] - \log[C(t_1)]}. \tag{3.12}$$

The lifetime could also be obtained by calculating the flux

$$J(r) = \frac{\hbar}{2mi}\,[\psi(r)^*\nabla\psi(r) - \psi(r)\nabla\psi^*(r)]. \tag{3.13}$$

For a pure resonant state the flux should be asymptotically coordinate independent, thus $J \propto \tau_v$.

In the present one-channel calculations, the computed lifetimes using Eq. (3.12) are 174 ns, 7.4 ns, and 13.7 ps for the $v=0,1,2$ levels, respectively, in the K_2 long-range well. The marked difference between the time constants of $v=0,1$ clearly reflects that the uppermost level is the most sensitive to the tunneling through the barrier, which is the only decay process in the one-channel model. In such a model the $v=0$ level may be considered as a true bound state. The $v=2$ level is a resonance lying slightly above the barrier, and decaying with a much smaller lifetime.

The real time filtering procedure is different from the time-energy filter used to locate resonances by Baer[42] and Mandelstam *et al.*[43] It has the advantage that the procedure directly relates to our intuition of the behavior of a metastable state.

The time filtering procedure could well be implemented from a wave function obtained by the FGH method. More generally, we would like to put emphasis on the ''interconnectivity'' between the different steps of the method presented here, as illustrated by the diagram in Fig. 8: each filtering step (in energy or in time) might well be stopped at any arbitrary time step (imaginary or real), and the resulting wave function then is used as an input for the next filtering procedure, or for the Krylov diagonalization process.

IV. RESULTS

Section III was devoted to the presentation of our methods for calculating energies and lifetimes of resonant states, and illustrated using a single potential picture of the molecular system. Actually, we have shown in Fig. 2 and Sec. II that two potentials should be considered. We now present two-channel calculations in both FGH and FDM approaches for the K_2 and Rb_2 molecules only. Indeed, no bound levels have been found for Na_2, despite the presence of a well in the upper adiabatic curve: for this molecule, the weakness of the spin–orbit coupling does not allow one to consider Hund's case c as a good approximation for the description of the electronic states.

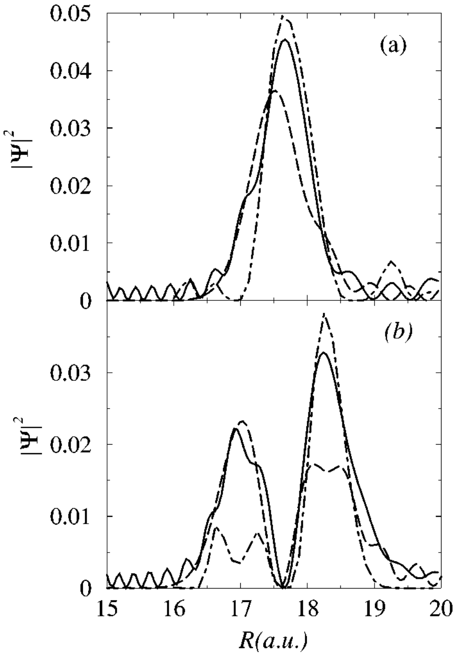

FIG. 9. Probability densities for the (a) $v=0$ level, (b) $v=1$ level in the $0_g^+(P_{3/2})$ potential curve in K_2, in a two channel model. Full line: FGH, [15–20 a.u.] grid, dashed line: FGH, [6–30 a.u.] grid, dot-dashed line: FDM.

A. Quasibound states of K_2

Only two states $v=0,1$, with a wave function located mainly in the outer well of the $0_g^+(P_{3/2})$ potential, are found within the two-channel FGH approach. As shown in Fig. 9 for both grids defined above, the wave functions are strongly perturbed by the continuum of the $0_g^+(P_{1/2})$ potential, and one may expect strong predissociation effects, with a lifetime substantially smaller than for the one-channel model. The

TABLE III. Energies E (in cm^{-1}), relative to the $(4s+4p)$ asymptote, rotational constants B_v (in cm^{-1}), and lifetimes (in ps) computed in a two-channel model, for the $v=0,1,2$ levels in the outer well of the $0_g^+(P_{3/2})$ potential curve in K_2. The initial guesses ϵ for the energy and the dispersion D (in cm^{-1}) in the FDM are also reported. We used 180 time steps of 0.5 ps in filtering, before diagonalization.

Method		$v=0$	$v=1$	$(v=2)$
FGH				
[6–30 a.u.] grid	E	294.95	312.88	⋯
[15–20 a.u.] grid	E	293.63	312.32	⋯
	B_v	9.9×10^{-3}	9.7×10^{-3}	⋯
FDM	E	293.18	313.64	325.47
$\epsilon=310$	D	0.45	0.004	0.31
	τ_v(ps)	20.4	17	4.6

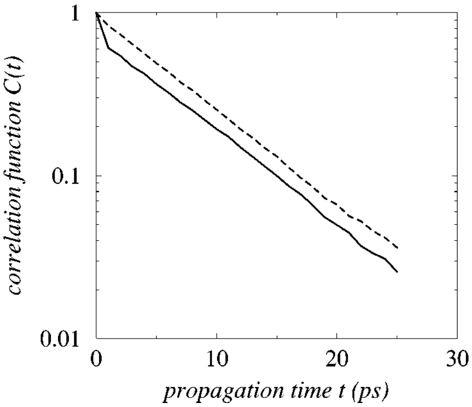

FIG. 10. Correlation function $C(t)$ (on a logarithmic scale) for the $v=0$ and $v=1$ in the outer well of the $0_g^+(P_{3/2})$ potential curve in K_2 (two channel calculation).

corresponding energies and rotational constants are reported in Table III. The energies differ only slightly from those of Table II. Let us note that the size of the grid is a more critical issue than in the one-channel calculations: indeed, the density of continuum states for the $0_g^+(P_{1/2})$ potential increases with the size of the grid.

This latter remark also has consequences on the way to run the calculation within the FDM framework. Starting from an initial value ϵ, the value of the dispersion is no longer a good criterion to stop the filtering procedure: the expected bound state now being strongly mixed with the continuum of the $0_g^+(P_{1/2})$ channel, we obtain larger values for the dispersion. But for some choices of the initial value ϵ, deduced from the one-channel calculations, the final dispersion for the bound states deduced after diagonalization of the Krylov space is now excellent. Therefore we proceed via successive trials for the number of filtering steps N_τ; the results displayed in Table III have been found with $\epsilon=310\ \mathrm{cm}^{-1}$, after $N_\tau=180$ steps with a step size of 0.5 ps and with $n_{\mathrm{Kryl}}=5$. They are very similar to those of the FGH approach.

The real time propagation of the $v=0$ and $v=1$ FDM wave functions provides the correlation functions drawn in Fig. 10. Both levels are decaying much faster than in the one-channel model, and with comparable time constants (20.4 and 17 ps for $v=0$ and $v=1$, respectively). The decay through predissociation in the $0_g^+(P_{1/2})$ continuum is now the dominant process, and energy of both levels are close enough to be perturbed in a similar way by the coupling term. Let us note that the $v=0$ level exhibits a short-lived component (with a time constant of 8.5 ps), probably due to a small defect of the filtering procedure (the dispersion is larger for this level, see Table III). In contrast, the lifetime of the $v=2$ resonance is now found equal to 4.6 ps. Further work should sort out whether this figure is the real lifetime or still contains errors due to the filtering procedure.

B. Quasibound states of Rb_2

As the $Rb_2(0_g^+(P_{3/2}))$ outer well is deeper than in K_2, the number of bound states obtained in the one-channel model is larger. The energies of the 11 levels computed by the FGH method are reported in the first column of Table IV. A grid ranging from $14a_0$ to $22a_0$, with a step size of $0.07a_0$ was used. The position of the levels is only slightly modified when two-channel calculations are performed. Indeed, due to the value of the fine structure constant, four time larger than for K_2, Hund's case c representation is a good approximation for the two 0_g^+ electronic states. At the avoided crossing, the two potential curves stay far apart, so that the radial coupling is very small (see Fig. 2).

Implementing the FDM method is more delicate than in the K_2 calculations. We used a grid similar to the FGH grid above. We had to filter the vibrational levels by groups ($v=0-2$, $v=3-6$, $v=7-10$) with different initial guesses ϵ, to reach a small dispersion on their energies. It is striking that for the one-channel calculations, both methods yield equivalent results within a few $0.01\ \mathrm{cm}^{-1}$, except for the two uppermost levels. This is reflected also in the very small value of the dispersion. The $v=8,9,10$ levels are decaying by

TABLE IV. Energies E (in cm^{-1}) relative to the $(5s+5p)$ asymptote, and rotational constants B_v (in cm^{-1}), computed within both FGH and FDM approaches, in a one-channel (FGH-1, FDM-1) and two-channel model (FGH-2, FDM-2), for the $v=0$ to $v=10$ levels in the outer well of the $0_g^+(P_{3/2})$ potential curve in Rb_2. Lifetimes for the quasibound states yielded by FDM-2 are also reported. The number of filtering time steps N_τ, the initial guess ϵ and the dispersion D (in cm^{-1}) in the FDM are also specified.

	FGH-1	FGH-2		FDM-1				FDM-2				
v	E	E	$10^3\times B_v$	N_τ	ϵ	E	D	N_τ	ϵ	E	D	τ_v
0	262.23	263.05	4.70	6	120	262.28	0.31	200	270	263.09	0.17	⋯
1	274.40	274.50	4.74	6	120	274.40	0.006	200	270	274.57	0.70	⋯
2	285.32	285.36	4.76	6	120	285.32	0.06	200	270	285.35	0.47	⋯
3	295.42	295.64	4.77	100	310	295.42	0.02	200	310	295.67	0.14	⋯
4	305.04	305.34	4.77	100	310	305.04	0.04	200	310	305.37	0.17	⋯
5	314.19	314.44	4.75	100	310	314.19	0.04	200	310	314.46	0.17	⋯
6	322.80	322.90	4.71	100	310	322.80	0.03	200	310	322.92	0.20	⋯
7	330.70	330.64	4.63	200	340	330.70	0.03	150	330	330.97	0.64	⋯
8	337.53	337.53	4.50	200	340	337.51	0.06	250	340	337.63	0.64	2.6 ns
9	343.20	343.44	4.33	200	340	343.30	0.04	250	340	343.50	0.89	0.93 ns
10	348.13	348.42	4.16	200	340	348.04	0.04	250	340	348.76	0.51	54 ps

tunneling through the barrier, with lifetimes of 3 ns, 0.67 ns, and 40 ps, respectively.

When comparing the two-channel calculations, both methods are still found in very good agreement up to $v=6$, although the dispersion is now one order of magnitude larger. For the $v=7-10$ levels, the discrepancies between the two approaches are about $0.1\ \mathrm{cm}^{-1}$. This is easily interpreted since these uppermost levels have lifetimes shorter than 10 ns (see the last column of Table IV), and interact with the $0_g^+(P_{1/2})$ dissociation continuum. But the lifetimes are only slightly modified by the presence of this continuum (2.6 ns, 0.93 ns, and 54 ps, respectively), reflecting the adiabatic character of the coupling. Moreover, they are still larger than in the K_2 molecule.

In view of possible spectroscopic identification of these levels, we also display in Table IV their computed rotational constants $B_v=\langle 1/(2\mu R^2)\rangle$. The extremum predicted for the $v=3,4$ levels will be very sensible to the shape of the potential, and may be found slightly shifted towards neighboring levels in an experimental spectrum.

V. CONCLUSION

In the present work, we have investigated the possibility of populating bound or quasibound levels in the outer well of the 0_g^+ potential curves correlated to the first $ns+np(^2P_{3/2})$ asymptote of the alkali dimers. Wells exist for Na_2, K_2, and Rb_2, their depth ranging from 40 to $90\ \mathrm{cm}^{-1}$. The bottom of such wells is located $176-317\ \mathrm{cm}^{-1}$ above the dissociation limit, so that the excitation scheme should use a laser light markedly blue detuned from the atomic resonance frequency. Due to the location of the well, the possible bound states are embedded in the dissociation continuum of the $0_g^+(ns+np(^2P_{3/2}))$ potential curve. Moreover, radial coupling with the continuum states of the 0_g^+ potential curve located below and correlated to the $ns+np(^2P_{1/2})$ asymptote, has to be considered. The problem therefore deals with two continua.

We have used this system as a way of checking the accuracy and limitations of two different grid methods which have been developed in different physical situations and, to our knowledge, never been applied to a similar case. One method (Fourier grid Hamiltonian) is diagonalizing a numerical Hamiltonian directly computed on a grid. The other (filter diagonalization) uses a filter method based on a propagation technique in imaginary time, to generate approximate vibrational wave functions which are further improved by diagonalization in a Krylov subspace. We have performed both one-channel, and two-channel calculations considering the upper $0_g^+(^2P_{3/2})$ and lower $0_g^+(^2P_{1/2})$ Hund's case c potential curves. The lifetimes of the quasibound states have then been determined by propagation of the wavefunctions in real time.

No quasibound state is found in Na_2, as the fine structure coupling is too small for the Hund's case c picture to be valid. In the K_2 molecule, both methods give similar results in a one-channel approach where tunneling through the barrier is the only decay mechanism. Results are slightly different in the two-channel calculations, where the predissociation to the continuum of the lower lying $0_g^+(^2P_{1/2})$ curve is the dominant decay mechanism. The existence of two quasibound states is predicted, with lifetimes of the order of 20 ps. The treatment of a double continuum problem has been completed by study of a $v=2$-like level located just above the barrier $(0.2\ \mathrm{cm}^{-1})$. The 4.6 ps value found for the lifetime should be checked in further work. The agreement between one-channel calculations with both methods is also very good for Rb_2, with discrepancies smaller than $0.1\ \mathrm{cm}^{-1}$ on the energies. The first eight levels are true bound states, and are not perturbed by the coupling with the lower $0_g^+(^2P_{1/2})$ curve. The last three levels $v=8,9,10$ are predicted to be quasibound, with lifetimes varying from 30 ps to 2 ns.

As a conclusion, both methods seem well adapted to analyze such systems with intermediate long-range wells, if the required accuracy on the vibrational energies is around $0.1\ \mathrm{cm}^{-1}$. In the present state of potential curve calculations, better accuracy is not relevant.

Experimental work should investigate the possibility of populating the quasibound levels by photoassociation induced by a laser blue detuned from the resonance line. Another population scheme could be by direct bound–bound triplet transition in cold K_2 or Rb_2 molecules weakly attached to helium clusters (Refs. 44 and 45).

These quasibound levels can be used as an intermediate step in two-color experiments in a cold alkali sample.

ACKNOWLEDGMENTS

Helpful discussions with Mihaela Vatasescu are gratefully acknowledged. This work was made possible owing to the CNRS-MOSA bilateral franco-israeli cooperation agreement, which supported two two-weeks visits for F. M.-S. and O. D. at the Fritz Haber Center in Jerusalem, and from Université Paris-Sud, which supported a one month visit for G. P. in laboratoire Aimé Cotton.

[1] P. D. Lett, K. Helmerson, W. D. Philips, L. P. Ratliff, S. L. Rolston, and M. E. Wagshul, Phys. Rev. Lett. **71**, 2200 (1993).

[2] V. Bagnato, L. Marcassa, C. Tsao, Y. Wang, and J. Weiner, Phys. Rev. Lett. **70**, 3225 (1993).

[3] J. D. Miller, R. A. Cline, and D. J. Heinzen, Phys. Rev. Lett. **71**, 2204 (1993).

[4] D. Leonhardt and J. Weiner, Phys. Rev. A **52**, R4332 (1995).

[5] H. Wang, P. L. Gould, and W. C. Stwalley, Phys. Rev. A **53**, R1216 (1996).

[6] W. C. Stwalley, Y. H. Uang, and G. Pichler, Phys. Rev. Lett. **41**, 1164 (1978).

[7] M. Movre and G. Pichler, J. Phys. B **10**, 2631 (1977).

[8] L. P. Ratliff, M. E. Wagshul, P. D. Lett, S. L. Rolston, and W. D. Philips, J. Chem. Phys. **101**, 2638 (1994).

[9] P. A. Molenaar, P. Van der Straten, and H. G. M. Heideman, Phys. Rev. Lett. **77**, 1460 (1996).

[10] R. A. Cline, J. D. Miller, and D. J. Heinzen, Phys. Rev. Lett. **73**, 632 (1994).

[11] L. Marcassa, S. Muniz, E. de Queiroz, S. Zilio, V. Bagnato, J. Weiner, P. S. Julienne, and K. A. Suominen, Phys. Rev. Lett. **73**, 1911 (1994).

[12] S. Zilio, L. Marcassa, S. Muniz, R. Horowicz, V. Bagnato, R. Napolitano, J. Weiner, and P. S. Julienne, Phys. Rev. Lett. **76**, 2033 (1996).

[13] V. Sanchez-Villicana, S. D. Gensemer, K. Y. N. Tan, A. Kumarakrishnan, T. P. Dinneen, W. Süptitz, and P. L. Gould, Phys. Rev. Lett. **74**, 4619 (1995).

[14] D. Hoffmann, S. Bali, and T. Walker, Phys. Rev. A **54**, R1030 (1996).

[15] M. Walhout, U. Sterr, C. Orzel, M. Hoogerland, and S. L. Rolston, Phys. Rev. Lett. **74**, 506 (1995).
[16] H. Katori and F. Shimizu, Phys. Rev. Lett. **73**, 2555 (1994).
[17] K. M. Jones, S. Maleki, L. P. Ratliff, and P. D. Lett, J. Phys. B **30**, 289 (1997).
[18] H. Wang, X. T. Wang, P. L. Gould, and W. C. Stwalley, Phys. Rev. Lett. **78**, 4173 (1997).
[19] R. Beuc, S. Milošević, M. Movre, G. Pichler, and D. Veža, Fizika (Zagreb) **14**, 345 (1982).
[20] F. H. Mies, C. J. Williams, P. S. Julienne, and M. Krauss, J. Res. Natl. Inst. Stand. Technol. **101**, 521 (1996).
[21] R. Kosloff, J. Phys. Chem. **92**, 2087 (1988).
[22] M. Monnerville and J. M. Robbe, J. Chem. Phys. **101**, 7580 (1994).
[23] O. Dulieu and P. S. Julienne, J. Chem. Phys. **103**, 60 (1995).
[24] R. Kosloff and H. Tal-Ezer, Chem. Phys. Lett. **127**, 223 (1986).
[25] A. D. Hammerich, J. G. Muga, and R. Kosloff, Isr. J. Chem. **29**, 461 (1989).
[26] D. Neuhauser, J. Chem. Phys. **93**, 2611 (1990).
[27] M. R. Wall and D. Neuhauser, J. Chem. Phys. **102**, 8011 (1995).
[28] S. Magnier, Ph. Millié, O. Dulieu, and F. Masnou-Seeuws, J. Chem. Phys. **98**, 7113 (1993).
[29] S. Magnier and Ph. Millié, Phys. Rev. A **54**, 204 (1996).
[30] M. Foucrault, Ph. Millié, and J. P. Daudey, J. Chem. Phys. **96**, 1257 (1992).
[31] M. Marinescu and A. Dalgarno, Phys. Rev. A **52**, 311 (1995).
[32] N. Spiess, Ph.D. thesis, Fachbereich Chemie, Universität Kaiserslautern, 1989.
[33] R. Meyer, J. Chem. Phys. **52**, 2053 (1970).
[34] R. Kosloff, Annu. Rev. Phys. Chem. **45**, 145 (1994).
[35] G. Ashkenazi, R. Kosloff, S. Ruhman, and H. Tal-Ezer, J. Chem. Phys. **103**, 10005 (1995).
[36] D. Neuhauser, J. Chem. Phys. **100**, 5076 (1994).
[37] C. Lanczos, J. Res. Natl. Bur. Stand. **45**, 255 (1950).
[38] R. Heather and H. Metiu, J. Chem. Phys. **86**, 5009 (1987).
[39] D. Neuhauser and M. Baer, J. Chem. Phys. **92**, 3419 (1990).
[40] G. Balint-Kurti and A. Vibok, in *Numerical Grid Methods and their Application to Schrödinger's Equation*, edited by C. Cerjan (Kluwer Academic, 1993), p. 412.
[41] R. H. Bisseling, R. Kosloff, and J. Manz, J. Chem. Phys. **83**, 993 (1985).
[42] R. Baer, Y. Zeiri, and R. Kosloff, Phys. Rev. B **54**, R5287 (1996).
[43] T. P. Grozdanov, V. A. Mandelstam, and H. S. Taylor, J. Chem. Phys. **103**, 7990 (1995).
[44] F. Stienkemeier, J. Higgins, W. E. Ernst, and G. Scoles, Phys. Rev. Lett. **74**, 3592 (1995).
[45] F. Stienkemeier, W. E. Ernst, J. Higgins, and G. Scoles, J. Chem. Phys. **102**, 615 (1995).